Thermal and composting degradation of EVA/Thermoplastic starch blends and their nanocomposites

Valentina Sessini [a, b, **], Marina P. Arrieta [c], Jean-Marie Raquez [a], Philippe Dubois [a], José M. Kenny [b], Laura Peponi [c, *]

[a] Laboratory of Polymeric and Composite Materials, University of Mons — UMONS, Place du Parc 23, 7000, Mons, Belgium
[b] Dipartimento di Ingegneria Civile e Ambientale, Università di Perugia, Strada di Pentima, 05100, Terni, Italy
[c] Instituto de Ciencia y Tecnología de Polímeros, ICTP-CSIC, calle Juan de la Cierva 3, 28006, Madrid, Spain

ARTICLE INFO

ABSTRACT

In this work, the thermal degradation and the disintegrability under composting conditions of melt-processed blends based on ethylene-vinyl acetate and thermoplastic starch, EVA/TPS, as well as their nanocomposites, reinforced with natural bentonite, were studied. A special emphasis was first put on the influence of starch on the morphology, thermomechanical properties and hydrophilicity of these blends before composting analysis. In fact, the materials were characterized in terms of morphological, mechanical, thermal and structural properties as well as wettability performance, obtaining information about the immiscibility of the blends and their compatibilization when natural bentonite is used. The thermal stability of starch was increased according with the EVA content in the blend, while the compatibility between both polymeric phases was increased by adding the nanoclays. Consequently, the disintegration under composting condition at laboratory scale level of the obtained materials was conducted and the thermal and chemical-structural properties as well as the surface microstructural changes of recovered samples at different stages of disintegration were studied. Disintegration tests showed that EVA/TPS blends and their nanocomposites presented positive interactions, which delay the disintegration of TPS matrix in compost, thus improving TPS stability. Moreover, blending biodegradable polymers such as TPS with non-biodegradable polymers like EVA leads to the increase of compostable polymer percentage in partially-degradable materials giving a possible solution for the end-life of these materials after their use.

© 2018 Published by Elsevier Ltd.

1. Introduction

Worldwide demand for plastic has being increased in several applications in the last years. It has been estimated that 275 million metric tons of plastic waste was generated in 192 coastal countries in 2010, with 4.8—12.7 million metric tons being directly disposed in oceans [1]. Additionally, the cumulative quantity of plastic waste that could get introduced into ocean from land is predicted to increase by an order of magnitude by 2025 [1]. In order to reduce the environmental problems caused by plastic wastes, the development of new materials based on renewable resources such as natural biodegradable polymers has been a challenge in the last years, becoming a challenge for academic and industrial research [2,3]. The utilization of agricultural products in plastic application is considered as an interesting way to reduce surplus farm products and to consolidate their revenues for non-food applications [4]. In this context, starch can be an ideal sustainable alternative to petroleum-based plastics, mainly due to its abundance, renewability, biodegradability, non-toxicity and low cost [5]. Starch in its native form is widely used as a filler [6], but its melt-processing by conventional methods, in presence of plasticizers such as glycerol, lead to a thermoplastic matrix (thermoplastic starch, TPS) useful for many application such as in packaging and biomedical field [7—9]. In fact, plasticized starch can be industrially processed with the traditional melt-processing methods such as extrusion, injection molding and film blowing [10]. However, there are several

* Corresponding author.
** Corresponding author. Laboratory of Polymeric and Composite Materials, University of Mons — UMONS, Place du Parc 23, 7000, Mons, Belgium.
E-mail addresses: valentina.sessini@umons.ac.be (V. Sessini), marrieta@ictp.csic.es (M.P. Arrieta), jean-marie.raquez@umons.ac.be (J.-M. Raquez), philippe.dubois@umons.ac.be (P. Dubois), jose.kenny@unipg.it (J.M. Kenny), lpeponi@ictp.csic.es (L. Peponi).

disadvantages that make its broad application unfeasible. Poor mechanical behavior and high water vapor permeability are the main drawbacks of starch-based materials [8]. Moreover, depending on the storage conditions of thermoplastic starches, recrystallization (retrogradation) leads to an undesired change in the thermo-mechanical performances of the final starch-based material [11]. In order to address the limitations of native starch-based materials, different modifications has been proposed in literature [12]. Among the principal achievements that can be obtained by starch modifications, we can find to decrease in retrogradation, improvement in film processability and increase in hydrophobicity. The most common methods used to modify starches can be classified into four broad areas: chemical, physical, enzymatic, and genetic modifications [13–16]. Between all modification methods it is important to notice the environmental friendly character of physical modifications, as they do not involve any severe chemical conditions.

An interesting approach to improve the properties and the stability during the application of thermoplastic starch is by blending with other hydrophobic polymers such as polyethylene (PE) [17] and polycaprolactone (PCL) [18]. Indeed, starch can be used together with a fully biodegradable synthetic polymers, producing biodegradable blends of low costs or also blended with synthetic non-biodegradable polymer [19,20]. Ferri et al. reported that industrial TPS enables easy processing and provide high ductile materials with improved elongation at break, reduced retrogradation effects and improved thermal stability [21]. TPS has been blended with polylactic acid (PLA) [22], polyhydroxybutyrate (PHB) [23], polypropylene (PP) [24] and hydrolyzed ethylene-vinyl acetate [25] among other polymers.

In general, the processing of polymer blends is an interesting goal for both research groups and industrial companies because of it is an easy, low-cost, scalable way to enhance the properties of pristine polymers. In general, commercial polymer blends are immiscible presenting two separated phases. However, still in this case, they have very useful properties [4]. The final properties of the blends are strongly affected by the phase-separated morphology, and thus controlling this morphology can lead to synergistic properties for the final blend [26]. One of the main drawbacks of using TPS as co-component in polymer blends is its poor miscibility with the other polymeric components. The good compatibilization and miscibility of blends can be achieved by combining with nanofillers, due to the decrease of the total free energy of mixing [27,28]. Indeed, the preparation of nanocomposites, using low percentages of inorganic fillers (commonly less or equal to 1%), is among the routes to both, improve some of the properties of biodegradable polymers and compatibilizing immiscible blends [29]. Nanoclays are one of the most used inorganic nanofiller used to obtain polymer based nanocomposites. Among them, bentonites are of particular importance not only due to environmental and economic relevance, but also due to their chemical and physical properties, characterized for a moderate negative charge [30]. Moreover, the polar character of natural bentonite ($CLNa^+$) can be an advantage to give positive interactions with polar polymeric matrices when used as fillers in the processing of nanocomposites.

Copolymers of ethylene-vinyl acetate (EVA) are a class of widely used polymers, with a variety of industrial applications such as flexible packaging, membranes, cable and wire, hose and tube, photovoltaic encapsulants, footwear and biomedical applications [31–33]. However, in many cases, their applications are limited due to their low tensile strength, thermal stability, high flammability and non-degradability. Da Róz et al. [25] reported the processing of compatible EVA/TPS blends with low EVA content (max. 10 wt %) modified by hydrolysis of 50% and 100% of the vinyl acetate groups. This study shows that the addition of only 2.5 wt % of hydrolyzed

EVA was able to improve the mechanical, thermal and water absorption characteristics of TPS. Furthermore, Prinos et al. [34] studied the effect of EVA, as compatibilizer, on the mechanical and thermal properties of TPS/low density polyethylene blends. They reported that increasing the EVA content in the blend the mechanical and thermal properties were improved.

In our previous works [35,36], multi-responsive EVA/TPS blends and their respective nanocomposites reinforced with $CLNa^+$ were processed by melt compounding. The role of natural bentonite was to act as compatibilizer within these blends. Interestingly, thermally- and humidity-activated shape memory properties were highlighted, together with good thermal, mechanical and dynamic mechanical properties.

For the best of our knowledge, the disintegration under composting conditions of EVA/TPS blends and nanocomposites has not been reported in literature. In the present work, we focus on the thermal stability and the degradation under composting condition at laboratory scale level of EVA/TPS blends and their nanocomposites reinforced with $CLNa^+$, obtained by melt processing. Firstly, special emphasis was put on the influence of starch on the thermomechanical properties and hydrophilicity of these blends before composting analysis. Consequently, the disintegration under composting condition at laboratory scale level of the obtained materials was conducted and the morphological, thermal and structural analysis of such degraded material is reported here. The changes on the morphology of the blends and their nanocomposites, the hydrophilic character of TPS phase and its biodegradability on the resulting compostability properties of EVA/TPS based materials was studied with the main objective to have information about the end-life of these materials for potential industrial applications (i.e.: agricultural mulch films, food packaging, etc.).

2. Experimental

2.1. Materials

Native pea starch was obtained from Cosucra groupe Warcoing SA, Belgium, with a dry content of 85 wt %, including 60.7 wt % amylopectin, 35.7 wt % amylose, 3.4 wt % fiber, and 0.24 wt % protein, as determined by colorimetric methods and Prosky and DUMAS methods [37]. Starch was used as received. Commercial EVA copolymer with 19 wt % of vinyl acetate (VA) content was purchased from Exxon Mobil Chemical Company. Glycerol (purity 97%) was purchased from VWR International and was used as starch plasticizer. Commercial natural bentonite, Cloisite-Na$^+$ ($CLNa^+$) was purchased from BYK Additives and Instruments. Its dimensions are typically ranging from 2 to 13 μm.

2.2. Starch-based blends and nanocomposites processing

Two different blends with different TPS content, i.e. 40 wt % and 50 wt %, were processed, as well as their nanocomposites reinforced with 1 wt % of $CLNa^+$. The formulations of the blends and the amount of the nanofiller added in the polymeric matrix were chosen in function of the better thermal- and humidity-responsiveness of the materials as reported in our previous works [35,36]. The processing method used was reported elsewhere [35]. In summary, the materials were processed in two steps:

- Thermo-mechanical destructuration of native starch granules with liquid glycerol and distilled water (in the wt ratio of 100:25:20) was performed in a Brabender® internal kneader (for 3 min at 110 °C with a rotor speed of 100 rpm) in order to obtain thermoplastic starch.

- Melt-blending of TPS with commercial EVA with a twin-screw DSM microcompounder for 5 min at 160 °C with a screw speed of 125 rpm.

Therefore, the blends with 40 and 50 wt % of TPS were obtained and named B40TPS and B50TPS, respectively. When the nanocomposites had been processed, CLNa$^+$ nanoclays were used as nanofillers and were prior mixed with TPS through melt intercalation method. Two different nanocomposites, with 1 wt % of CLNa$^+$ were obtained, named B50TPS + 1% CLNa$^+$ and B40TPS + 1% CLNa$^+$. The extruded blends and nanocomposites were successively thermo-compressed in a hot press for 5 min at 160 °C at 200 bars in order to obtain films to carry out their characterization.

2.3. Disintegration under composting conditions

The disintegrability test under aerobic composting conditions mediated by thermophilic bacteria was performed at laboratory scale level [38]. The materials were cut into square-shaped samples (15 mm × 15 mm) and they were contained in a textile mesh to allow their easy removal after composting test, but also allowing the access of moisture and microorganisms. They were buried at 4−6 cm depth in perforated plastic boxes containing a solid synthetic wet waste (10% of compost (Compo, Spain), 30% rabbit food, 10% starch, 5% sugar, 4% corn oil, 1% urea, 40% sawdust and approximately 50 wt % of water content) and were incubated at aerobic conditions (58 °C) to get information about the degradation of EVA/TPS blends and nanocomposites produced by thermophilic bacteria. The aerobic conditions were guaranteed by periodical mixing of the solid synthetic wet waste. One sample of each formulation was recovered from the disintegration container at different times (1, 11, 18, 25, 32, 39 and 56 days for TPS while all the other samples at 1, 11, 18, 56, 120 and 150 days) following previous reported procedures [39−42]. The film samples were then cleaned with distilled water, dried in an oven at 37 °C during 24 h, and reweighed. The disintegration degree was calculated by normalizing the sample weight, at different days of incubation, to the initial weight, while photographs were taken to all samples once extracted from the composting medium.

2.4. Characterization techniques

2.4.1. Characterization of EVA/TPS based blends and nanocomposites

The thermal properties were investigated by Differential Scanning Calorimetry (DSC) analysis. The dynamic DSC measurements were performed in a Mettler Toledo DSC822e instrument, under nitrogen flow (30 ml min^{-1}). Samples of about 10 mg were sealed in aluminum pans. Thermal cycles were composed by the following "heat/cool/heat" procedure: heating at 10 °C min^{-1} from room temperature (RT) to 150 °C, cooling at 10 °C min^{-1} to −80 °C and heating again at 10 °C min^{-1} to 150 °C.

Mechanical properties were determined using an Instron Universal Testing Machine at a strain rate of 150 mm min-1. Tensile test measurements were performed on 5 dog-bone specimens with a width of 2 mm, thickness of 0.60 mm and leaving an initial length between the clamps of 20 mm. From these experiments were obtained the Young Modulus, as the slope of the curve between 0% and 2% of deformation, the elongation at break and the maximum stress reached. Samples were conditioned at 59% of relative humidity (RH) for 1 week at RT.

SEM micrographs of the cryo-fracture surface of the blends and their nanocomposites, were obtained by Scanning Electron Microscopy (SEM PHILIPS XL30 with a tungsten filament) in order to study their morphology and the compatibility of the two polymers in the blends and their nanocomposites. The polymer samples were frozen using liquid N$_2$ and then cryo-fractured. All the samples were gold/palladium coated by an automatic sputter coated Polaron SC7640. Field Emission Scanning Electron Microscope (FE-SEM, Hitachi S8000) in transmission mode was used to study the melt intercalation of the polymer and to observe the filler dispersion in the nanocomposites.

Thermogravimetric analysis (TGA) was carried out using a TA-TGA Q500 thermal analyzer on the specimens dried in a ventilated oven at 40 °C for three days. EVA/TPS blends and their nanocomposites were analyzed by dynamic mode using about 10 milligrams of sample from room temperature to 800 °C at 10 °C min^{-1} under nitrogen atmosphere with a flow of 60 mL min^{-1}. The initial degradation temperatures (T$_{5\%}$) were determined at 5% mass loss while temperatures at the maximum degradation rate (T$_{max}$) were calculated from the first derivative of the TGA curves (DTG).

Surface wettability of the EVA/TPS based films was studied through static water contact angle (WCA) measurements using a KSV Theta goniometer. The volume of the droplets was controlled to be about 7.0 μL and a charge coupled device camera was used to capture the images of the water droplets for the determination of the contact angles. The static WCA was determined by randomly putting 4 drops of distilled water with a syringe onto the film surfaces and the average values were used. Dynamic measurements of the WCA were also performed providing the hysteresis angle of the surface (WCAH). Advancing angle (ACA) was measured by adding water to the original static volume and the receding angle (RCA) by removing it. The WCAH was calculated as the difference between the advancing angle and the receding angle.

Attenuated total reflectance - Fourier transform infrared spectroscopy (ATR-FTIR) measurements were carried out with a Spectrum One FTIR spectrometer (Perkin Elmer instruments). Spectra of dried films (RH ≈ 10%) and conditioned films at 97% of RH were obtained in transmission mode at room temperature in the 4000-650 cm^{-1} region with a resolution of 4 cm^{-1} and 32 scans.

2.4.2. Characterization of degraded EVA/TPS blend and nanocomposites

For TGA of the samples after disintegration under composting conditions, the same procedure as for initial samples was used.

SEM micrographs of the surface of the blends and their nanocomposites, before and after disintegration under composting conditions, were obtained by Scanning Electron Microscopy (SEM PHILIPS XL30 with a tungsten filament) in order to study the differences in the surface microstructure of the blends and their nanocomposites after the disintegration under composting conditions. All the samples were gold/palladium coated by an automatic sputter coated Polaron SC7640.

ATR-FTIR measurements were carried out with a Spectrum One FTIR spectrometer (Perkin Elmer instruments) also for the sample after disintegration under composting conditions in order to study the structural changes during the degradation phenomenon. Spectra were obtained in transmission mode at room temperature in the 4000-650 cm^{-1} region with a resolution of 4 cm^{-1} and 32 scans.

2.5. Statistical analysis

Significance differences in the mechanical properties, WCA measurements as well as the TGA data among different extraction days were statistically analyzed by one-way variance analysis (ANOVA) by using Origin-Pro 8 software. Tukey's test with a 95% confidence level was used to identify what data groups were significantly different from others.

3. Results and discussion

3.1. Starch-based blends and nanocomposites properties

In our previous works [35,36], EVA/TPS blends and their nano-composites reinforced with 1 wt % of CLNa$^+$ were melt-processed giving particular emphasis on the thermally- and humidity-activated shape memory responsiveness and mechanisms.

However, blending TPS with EVA is a challenge with the aim to improve TPS performances in films manufacturing and use. Indeed, in this way is possible to decrease the high hydrophilicity of starch, that limits its industrial applications, and to improve its thermal stability as well as its mechanical properties. On the other hand, water absorption of bio-based materials is greatly important to promote microorganism attack and their disintegrability under composting conditions since the disintegration starts by a hydro-lysis process [39,43]. Thus, blending TPS with EVA is increasing the absorption of water of EVA based materials after using, leading to the promotion of their disintegrability under composting condi-tions. For this, particular attention was focused on the influence of the morphology and the compatibilization of the polymeric phases on the thermomechanical properties, wettability and disintegra-tion under composting condition behavior of EVA/TPS blends and their nanocomposites.

The thermal properties and the crystalline degree of EVA/TPS blends and of their nanocomposites were studied by DSC. A T_g about $-26\,°C$ was observed for pure EVA and it was related to the amorphous phase, consisting of amorphous PE and amorphous VA segments as previously reported in literature [44]. Pure EVA showed a $T_m = 86\,°C$ and a $T_c = 70\,°C$. No significant changes on the thermal properties were observed for the blends and their nano-composites compare with pure EVA. However, an increase on the degree of crystallinity was observed after adding 1 wt % of natural bentonite nanoclays in the system. Similar results are reported in literature for low amount of nanofillers, due to the nanoclay intercalation into the polymer chains acting as nucleating agent. Moreover, thermal transitions of TPS were difficult to be charac-terized because of their dependence on the humidity content in the samples and because they are overlapped by the broad melting pick of EVA phase. A deep study of the thermal properties of TPS has been showed in our previous work [36]. Due to the plasticizer effect of water, increasing the humidity content in starchy materials, the T_g values can decrease in a range of around 60 °C showing their high moisture sensibility.

To highlight the compatibilizing effect related with nanoclays, the FE-SEM technique was carried out in the nanocomposites (Fig. 1).

In particular, it is easy to notice that natural bentonite is pref-erentially located into TPS matrix, because of the hydrophilic character of the nanoclays and especially due to the polar interac-tion between the silicate layers and TPS as well previously demonstrated by Park et al. [45]. However, during the melt pro-cessing of the blend, the nanoclays migrated into the interface of the blend due to the interaction with the VA polar groups of EVA, increasing the interfacial adhesion between both polymeric phases.

The morphology of the blends and their nanocomposites were studied by SEM observation of the cryo-fracture section. The SEM images for all the samples studied are shown in Fig. 2.

The morphology observed in Fig. 2 shows that EVA/TPS blends are immiscible as expected. In the blends (Fig. 2a and b), TPS spherical microdomains with a non-homogeneous size distribution are dispersed into the EVA matrix. Moreover, phase debonding was observed indicating a poor adhesion between EVA and TPS phases. Very weak interfacial adhesion and immiscibility between TPS based blends have been already observed in the literature for PP-

Fig. 1. FE-SEM image of natural bentonite dispersion on B50TPS + 1% CLNa$^+$.

TPS blends [24] as well as in EVA/PLA blends [42]. However, in the case of nanocomposites, a more homogeneous size distribution of the TPS spherical microdomains was observed compared with the neat blends as well as a strong decrease of the phase debonding, indicating better compatibility between the different polymeric phases probably due to the addition of nanoclays. This behavior was already reported in literature for other blends based on PE or TPS [26,27]. Furthermore, the accu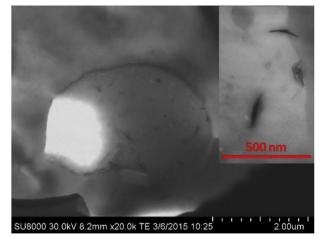mulation of nanoparticles at the polymer-polymer interface can change strongly the microstructure of immiscible polymeric blends improving the interfacial adhesion and suppressing the coalescence effect of the minor phase [46].

The morphological properties of the blends and their nano-composites are also reflected on their mechanical properties and thermal stability. The mechanical properties of all the materials have been tested and the results are showed in Supporting Infor-mation (Fig. S1). EVA showed the highest value of elongation at break compared with the other samples while TPS showed the lowest one. A quite low elastic modulus for EVA was observed, as expected for elastomers. TPS showed a typical elastic modulus (25 ± 8 MPa) of an amorphous polymer in the rubbery state because at room temperature and at RH = 59%, the material is above its T_g as it was showed in our previous work [36] and being in good agreement with values published in other works [47]. By increasing the amount of TPS in the blends, the materials become more brittle showing higher elastic modulus, lower maximum stress as well as elongation at break compared with pure EVA. Interestingly, a decrease of the elastic modulus (about 15%) was observed for the nanocomposites with respect to the corresponding neat blends, confirming the compatibilizer effect of nanoclays addition, rather than the reinforcement effect expected [48]. Similar results were reported from Samper-Madrigal et al. for PE/TPS blends compati-bilized with sepiolite nanofillers [28]. However, an increase of the maximum stress was showed for the nanocomposites compared with their corresponding neat blends, confirming the good dispersion of the nanoclays in the polymeric matrix.

The effect of EVA content on the thermal stability of TPS was studied as well as the effect of the improved EVA/TPS compatibility in the nanocomposites, due to the presence of natural bentonite as filler. The thermal degradation of EVA/TPS blends and their nano-composites, conditioned at 59% of RH, was studied by TGA under nitrogen atmosphere. In Fig. 3, the TGA and DTG thermograms for all the samples studied are showed and the main thermal param-eters obtained from these curves are summarized in Table 1.

Thermal degradation of EVA/TPS blends takes place in three main steps, as it was expected for immiscible blends, the first one
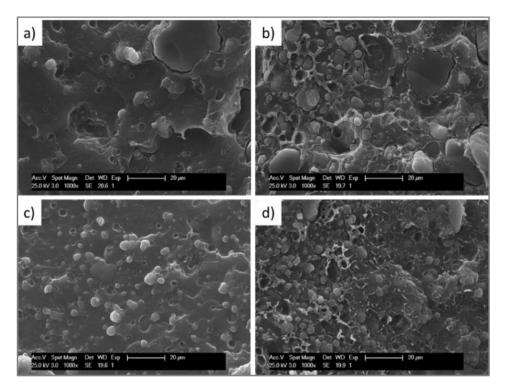
Fig. 2. SEM images of the cryo-fracture section of the EVA/TPS blends and their nanocomposites. a) B40TPS, b) B50TPS, c) B40TPS + 1% CLNa$^+$ and d) B50TPS + 1% CLNa$^+$.
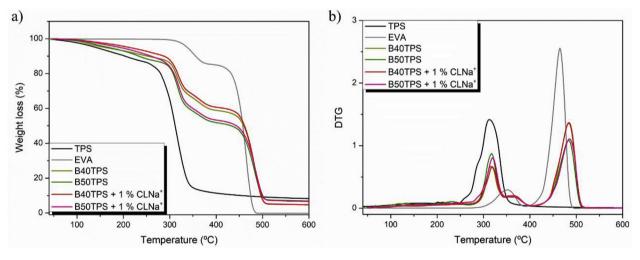

Fig. 3. TGA and DTG thermograms for all the samples conditioned at 50% of RH.

Table 1
TG and DTG values for all the samples conditioned at 50% of RH.

Sample	$T_{5\%}$ (°C)	T_{maxTPS} (°C)	$T_{maxEVAI}$ (°C)	$T_{maxEVAII}$ (°C)
EVA	338	—	352	465
TPS	141	313	—	—
B40TPS	159	317	368	484
B50TPS	160	317	363	484
B40TPS + 1% CLNa$^+$	212	319	367	484
B50TPS + 1% CLNa$^+$	191	320	369	486

due to TPS degradation and the others, due to EVA degradation. This result confirms the previous morphology observed by SEM analysis of immiscible EVA/TPS blends. In the TGA curves of neat TPS, blends and their nanocomposites is possible to observe a slightly weight

loss from around 80 °C due to the loss of bounded water in the film and low molecular weight compounds, as it was previously observed for starchy materials [49]. By blending EVA with TPS, the $T_{5\%}$ of TPS increased of about 20 °C as a consequence of TPS interaction with EVA. The improvement on the thermal stability is indicating that EVA inhibit the oxidation of biodegradable matrix as reported Fortunati et al. [42] in EVA-PLA blends. This effect was stronger for the nanocomposites, due to the compatibilizing effect of the nanoclay (Table 1). Similar results were reported in literature for EVA/TPS blends compatibilized by hydrolysis of vinyl acetate groups of EVA [25].

In literature, it was reported that the thermal decomposition mechanism of starch can be divided into different stages. The first stage is the physical dehydration, the water content depends on absorbed and bounded water in starch, as was observed in our case.

The second stage is the chemical dehydration and thermal decomposition [50]. Liu et al. [50] reported that the thermal degradation in starchy materials, start at around 300 °C with thermal condensation between hydroxyl groups of starch chains to form ether segments and liberation of water molecules and other small molecular species. They also reported that the dehydration of neighboring hydroxyl groups in the glucose ring also occurred, resulting in the formation of C-C bonds or breakdown of the glucose ring with the formation of aldehyde end groups at the same time. Fig. 3b shows that the first step of degradation had its T_{max} at around 310−320 °C (T_{maxTPS}) in good agreement with literature data [51]. A slight shift towards higher temperatures of T_{maxTPS} was observed for the blends (B40TPS and B50TPS) and much more for their nanocomposites, compare to neat TPS. This behavior is probably due to the positive interaction between EVA and TPS, according to the literature [25]. In the second step, the first EVA degradation process occurs in the range of 310−380 °C, through deacylation with elimination of acetic acid and the formation of double bonds. At temperatures higher than 400 °C, thermal degradation of the ethylene-co-acetylene random copolymer, resulting from deacylation, takes place. The weight loss curves of the blends and their nanocomposites displayed a slight stabilization of about 20 °C compare to neat EVA, as it is possible to easy notice in Table 1 for $T_{maxEVAI}$ and $T_{maxEVAII}$. Nguyen et al. reported an increase of about 30 °C of LLDPE thermal decomposition on LLDPE/TPS blends because the starch decomposition products are able to protect the polymer from heat degradation [27].

In Fig. 4, the normalized ATR-FTIR spectra of neat EVA, TPS and their blends, conditioned at different values of relative humidity, are reports since starchy materials are high water sensitive materials and, thus, structural changes can occur as a consequence of high water presence. Moreover, a comparison between the blends and their respective nanocomposites conditioned at high RH value (97%) is showed.

The ATR-FTIR spectra of neat EVA (Fig. 4a) shows a broad peak in the region of 3700-3000 cm^{-1} related to the -OH stretching, which increased in intensity under humidity conditions due to hydrogen bonding interaction between the carbonyl group in vinyl acetate and water. Two bands between 2950 cm^{-1} and 2850 cm^{-1} are associated with asymmetric and symmetric C-H stretching of the methylene group (-CH$_2$-), respectively. A band at 1738 cm^{-1} corresponds to the asymmetric stretching of the carbonyl group (−C=O), together with a small band at 1650 cm^{-1} due to the terminal trans-vinylene double bond (C=C) and another band at 1465 cm^{-1} due to the methylene stretch (CH$_2$). At 1156 cm^{-1} the band is ascribed to C-O-C stretch mode [42,52].

The main ATR-FTIR peaks of neat TPS (Fig. 4b) were the stretching vibration mode of the hydrogen-bonded -OH groups of starch (3000-3700 cm^{-1}) and the bending mode of the same groups (1642 cm^{-1}) [25,53]. Both bands increased with humidity (RH = 97%) due to the strong starch -OH groups interactions with water. Similarly, these two bands increased in EVA/TPS blends (Fig. 4c and d), showing particular higher intensity in the case of higher amounts of TPS (B50TPS) (Fig. 4d). In fact, EVA and TPS are able to establish hydrogen bonding interactions between the carbonyl group of vinyl acetate and -OH groups of starch as it was previously reported in literature where EVA was used as compatibilizer between LDPE and starch [34]. In B50TPS it was also observed an increased intensity of the bands attributed to the anhydroglucose ring O-C stretch (1020 cm^{-1}) [54].

Fig. 4e and f show the ATR-FTIR spectra of B40TPS and B50TPS blends and their nanocomposites, respectively, exposed to high humidity conditions (RH = 97%). Bentonite nanoclays have a characteristic absorption band at 1040 cm^{-1} ascribed to the stretching of Si−O−Si groups forming the crystalline tetrahedral structure of the clay layers [55]. However, it is difficult to observe the clay in the FTIR spectra in clay-based nanocomposites due to the small amount of clay in relation to the polymer phase and the overlap of the clay and starch bands [55,56]. The stretching vibration mode of the hydrogen-bonded -OH groups of starch (3000-3700 cm^{-1}) as well as the -OH bending mode (1642 cm^{-1}) increased in B40TPS + 1% CLNa$^+$ nanocomposite with respect of B40TPS blend (Fig. 4e), due to the already commented strong starch -OH groups interactions with water. Different behavior was observed in B50TPS+ 1% CLNa$^+$ nanocomposite in which these two bands decreased by showing reduced hydrogen-bonded interaction of starch matrix with water. This, suggests that starch matrix is better interacting with natural bentonite and consequently with EVA at this blend proportion (EVA: TPS 50:50 + 1% CLNa$^+$). This results are in good agreement with FE-SEM results and with those previously reported by Sessini et al. [36].

Surfaces wettability was studied in order to get information regarding the modification of the degree of the polymer surfaces hydrophobicity/hydrophilicity after blend and nanocomposites processing [57]. The contact angle between liquids such as water, and solid surfaces is based on the thermodynamic equilibrium between liquid, solid and vapor phases [20]. Indeed, the Young's equation defines the contact angle of a liquid drop on an ideal solid surface by the mechanical equilibrium of the drop under the action of three interfacial tensions: liquid-vapor, solid-vapor, and solid-liquid interfacial tensions [58]. A contact angle lower than 90° indicates that the wetting of the surface is favorable, and the fluid will spread over a large area on the surface. On the contrary, contact angles greater than 90° generally means that wetting of the surface is unfavorable so the fluid will minimize its contact with the surface and form a compact liquid droplet [59]. Fig. 5a reports the measured values of the water contact angle (WCA) for neat EVA and TPS, the blends and their respective nanocomposites. TPS exhibited the highest value and EVA the lowest one of WCA, while very similar intermediate values were observed for EVA/TPS blends (without significant differences for B50TPS, p < 0.05, and with significant differences for B40TPS, p > 0.05) and their nanocomposites (without significant differences p < 0.05), indicating apparently minor changes in the physicochemical characteristics of surfaces with the blending process of EVA with a high hydrophilic material such as TPS or by the introduction of a hydrophilic filler such as natural bentonite. The fact that the introduction of TPS slightly changed the wettability of EVA can be due to the formation of an EVA-rich surface during molding. In fact, EVA has lower viscosity than TPS, and thus it was probably able to flow around the TPS-rich phases and to encapsulate them, avoiding the exposure of starch phase on the surface of the samples. Similar results were reported from Perez et al. for LDPE/starch blends showing very similar values of contact angle for neat LDPE and its blend with 50 wt % of starch [20]. Moreover, the carbonyl groups of vinyl acetate from EVA phase and -OH groups of TPS are able to form hydrogen bonding interactions, as it was already commented in ATR-FTIR analysis [25]. Therefore, the -OH groups of starch are less available to interact with water at the surface. Unexpectedly, neat TPS showed a value of contact angle higher than 100°, as reported in Fig. 5a. Interestingly, this result can be due to the high amylose content of pea starch used in this work to obtain TPS matrix, which could lead to high surface roughness of TPS films [60]. In literature is reported that amylopectin films are totally amorphous and they are characterized by a smooth surface while, amylose films are semicrystalline giving rise to a rougher surface [61,62]. Moreover, Gutierrez et al. [63] claim that films derived from starches with a higher amylose content show a higher plasticizer−polymer compatibility compared with low amylose content starches. This
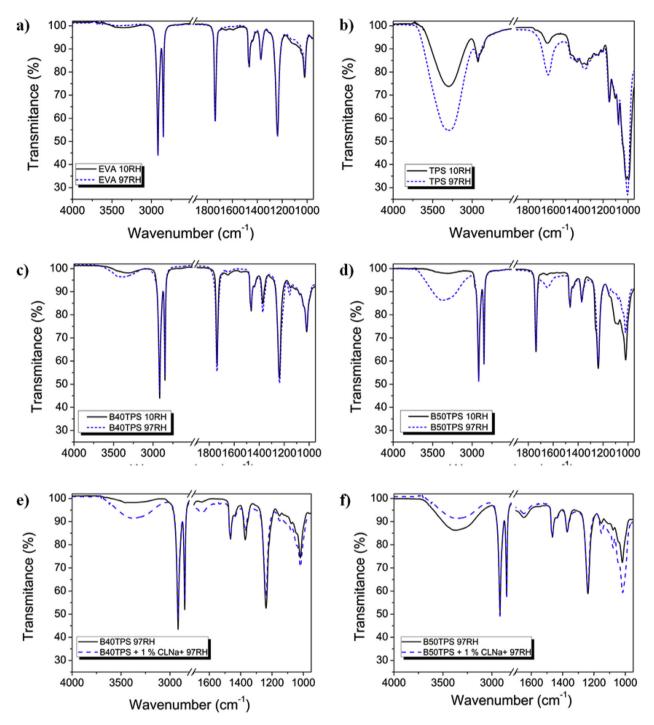
Fig. 4. ATR-FTIR spectra of dried films (RH ≈ 10%) and conditioned at 97% of RH a) EVA, b) TPS c) B40TPS and d) B50TPS. In addition, the spectra of B40TPS (e) and B50TPS (f) blends and their nanocomposites, respectively, exposed to high humidity conditions (RH = 97%).

allows to higher intermolecular hydrogen bonding between starch and plasticizer under the film surface, increasing the WCA values. Higher contact angle values were thus reported for films with a higher amylose content.

The water contact angle hysteresis (WCAH) was studied in order to study the changes on the surface wettability with dynamic measurements. The significance of contact angle hysteresis arises from surface roughness and/or heterogeneity. For heterogeneous surfaces, there exist domains that present barriers to the motion of the water drop/solid contact line [58].

Fig. 5b shows the average values of advancing contact angle (ACA) and receding contact angle (RCA) for neat TPS. It is easy to notice that after 3 cycles of dynamic measurement, neat TPS exhibited low values of both ACA and RCA, and thus more hydrophilic surface ($p > 0.05$). This is probably due to a reorganization of -OH groups in the TPS surface that became more available to form strong hydrogen bonding interactions with water compared to that in the dried material. On the other hand, neat EVA, EVA/TPS blends and their nanocomposites did not show strong differences ($p < 0.05$) between the dynamic measurement cycles (Fig. 5c).
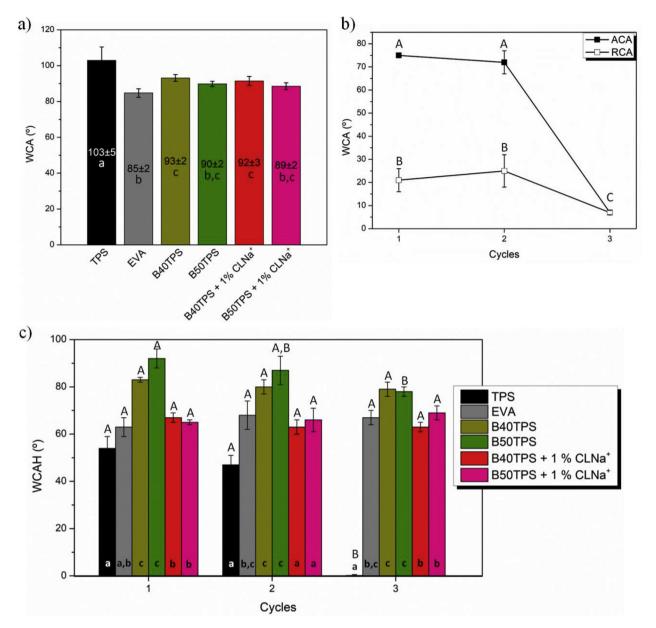
Fig. 5. Surface wettability: a) Static water contact angle for all the samples. [a-c] Different letters within columns indicate significant differences in WCA among samples ($p < 0.05$). b) ACA and RCA for TPS in the different cycles. [A-C] Different letters indicate significant differences in ACA and RCA TPS values among cycles ($p < 0.05$), c) WCAH for all the samples during different cycles. [A-B] Different letters within the same formulation in each cycle indicate significant differences in WCAH values ($p < 0.05$). [a-c] Different letters within samples in the same cycle indicate significant differences in WCAH ($p < 0.05$).

B50TPS showed a slight but significant ($p > 0.05$) decrease of the WCAH due to the higher amount of TPS present in the blend, while for its respective nanocomposite, the WCAH value slightly increase ($p < 0.05$) during the cycles. This fact is probably due to a major compatibility between TPS and EVA due to the presence of CLNa$^+$ [36] resulting in a lower availability of TPS —OH groups in the surface of the nanocomposite compare its respective blend.

3.2. Disintegrability under composting conditions of EVA/TPS based blends and nanocomposites

One of the most attractive issues about TPS-based materials is their intrinsic biodegradable nature. Composting as end-life options has gained considerable attention, where the plastic material undergoes degradation by biological processes (mainly microorganisms' enzymatic action), yielding to carbon dioxide,

new biomass and water (in the presence of oxygen), living no visually distinguishable materials [64]. Therefore, the disintegrability test under composting conditions at laboratory scale level was conducted in order to get information not only regarding the biodegradable character of these blends based on non-biodegradable and biodegradable materials, but also to better understand the compatibility between EVA and TPS matrices as well as the influence of natural bentonite on the improvement of their compatibility. Fig. 6a shows the visual appearance of pure materials, neat blends and their nanocomposites, recovered at different composting times. Polymers degradation mainly resumes started with a non-enzymatically hydrolysis, that leads into a significantly molar weight reduction followed by the enzymes action from the microorganisms present in the compost medium throughout the bulk of the polymeric matrix [43]. The biodegradation of starch-based polymers is a result of enzymatic attack at
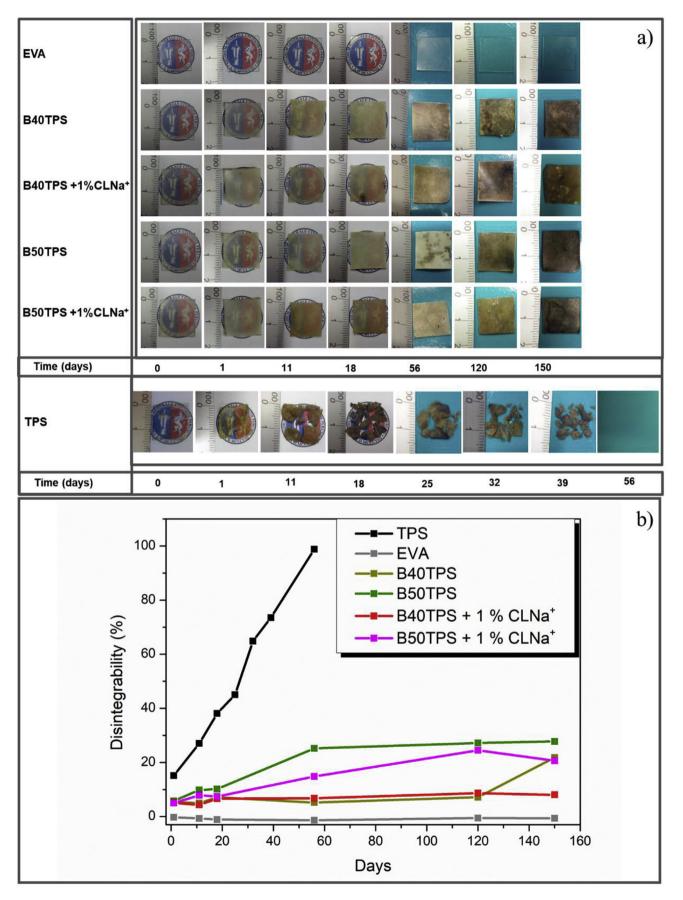
Fig. 6. Disintegration under composting conditions of all the materials, (a) visual appearance at different incubation time and (b) degree of disintegration as a function of time.

the glucosidic linkages of the long-chain sugar units, leading to their breakdown into oligosaccharides, disaccharides, and monosaccharides that are readily accessible to enzymatic attack [65]. While non-degradable EVA did not showed significant visible changes during composting, fully biodegradable neat TPS after 1 day in compost became yellowish and breakable and after 56 days virtually disappeared. The blends and their nanocomposites became opaque after 1 day while they were totally yellowish after 56 days and almost black after 150 days. The fact that materials became more opaque and the changes in color have been related with the beginning of the biodegradable polymeric matrices hydrolytic disintegration process, where a change in the refraction index of the materials is observed as a result of water absorption and/or presence of low molecular weight products formed due to the hydrolytic process [66]. It was clearly noticeable that apparent color changes were related to the TPS degradation stage. EVA/TPS blends first tended to get yellow until 18 days where there is still a remaining TPS matrix. Meanwhile, at higher testing times, (56 and 120 days) EVA/TPS blends tend to dark brown suggesting that starch matrix is being consumed by enzymatic microbial action, which accelerates the disintegration of polymer chain by producing small pores in the materials which weaken them [67]. Finally they were almost black at the end of the test (150 days). From the visual disintegration (Fig. 6a), it is expected that after 56 days TPS phase is almost disintegrated in compost. Thus, at high disintegration stages, in EVA/TPS blends and nanocomposites the formation of holes as well as the increased crystalline EVA fraction during degradation can be the responsible for the increased opacity in EVA-based samples, as it was already observed in EVA/biodegradable polymers blends [42] or there is a remaining amount of TPS in the blends. Therefore, to confirm the results from visual observations the disintegration degree (weight loss) as a function of composting time was calculated (Fig. 6b). As expected, EVA did not undergo significant changes during the whole incubation time, a slightly increase of its weight was observed due to the swelling phenomenon, taking place as a consequence of the water absorption under composting conditions. In this work, as reveled WCA measurement, EVA was the most hydrophilic sample. On the other side, neat TPS showed a high degree of disintegration, reaching 100% of disintegrability in less than 60 days. In the case of the blends, it was observed that they lost around 22% in B40TPS and around 28% in B50TPS of their initial weight at the end of the composting test, suggesting that there is a remaining fraction of TPS in the blends. At the composting temperature (between 50 °C and 60 °C) and under moisture, TPS can suffer aging phenomenon leading to long-chain amylose recrystallization that is accelerated by the presence of glycerol and high amounts of water [68]. This fact suggests that recrystallization renders the starch less available for enzymatic degradation decreasing the disintegration rate of starch. Concerning the kinetics of the disintegration, it should be mentioned that B50TPS blend and its nanocomposite was disintegrated faster than the materials based on B40TPS, due to the higher amount of biodegradable TPS in B50TPS based materials that promotes higher disintegration. Moreover, the higher amount of EVA in B40TPS can increase the encapsulation effect of starch dispersed domains hindering their degradation. Regarding the weight loss (Fig. 6b) of the blends and their nanocomposites it is easy to note that for the blend containing 40 wt % of TPS there were small differences compared with its respective nanocomposite, B40TPS + 1% CLNa$^+$. Indeed, both materials reached a maximum of about 9% of disintegrability in 120 days. Different behaviors was somehow observed for the blend containing 50 wt % of TPS, where the weight loss resulted slightly faster for B50TPS than the weight loss of its corresponding nanocomposite (B50TPS + 1% CLNa$^+$). This

may be due to the better compatibility observed in nanocomposites with 50 wt % of TPS (B50TPS + 1% CLNa$^+$) than that with 40 wt % of TPS (B40TPS + 1% CLNa$^+$) as it was already shown in FTIR analysis and previously reported by Sessini et al. [36] where the humidity responsiveness of B50TPS was higher than that of its respective nanocomposite. Meanwhile, B50TPS allowed greater accessibility of starch matrix to water and further to microorganisms attack. In nanocomposites, the presence of the filler hinders the molecular mobility of polymeric chains, and thus delays the TPS disintegration process. In fact, lesser disintegration degrees were observed in the nanocomposites at the end of the composting test (8% in B40TPS + 1% CLNa$^+$ and around 20% in B50TPS+ 1% CLNa$^+$), confirming that the compatibilizer effect of natural bentonite is protecting the TPS polymeric matrix from the microorganism attack [69]. In addition, it is known that nanoparticles can limit the water diffusion by the increase in barrier properties and consequently delay the hydrolysis process and further the enzymatic degradation [39].

All these results show that partially biodegradable blends were successfully obtained, since only the biodegradable starch matrix in considered to be disintegrated, showing higher values of disintegrability with higher TPS content, i.e.: higher than 20% for B50TPS. Similarly, Fortunati et al. [42] studied the disintegrability under composting conditions of EVA-PLA based blends and concluded that the amount of material at the end of the composting test represents the not degradable EVA fraction of the blends, while only the biodegradable PLA matrix was disintegrated.

The morphological changes due to the disintegration under composting conditions were studied from the collected specimens of materials before and after different degradation times by SEM micrographs and are shown in Fig. 7.

The films surface of the neat materials (Fig. 7a and c) was smooth before exposing to composting medium. Meanwhile, the film surface of the blends and their nanocomposites before the degradation test (Fig. 7g, k, o and s) appeared less homogeneous and with higher roughness, compared with that of EVA. Accordingly with WCA results, film based on starch with high amylose content are characterized by high roughness. Rindlav-Westling and Gatenholm [70] studied the surfaces of pure amylopectine and amylose films reporting that the surface (by SEM) of amylopectin films was very smooth, whereas that of amylose films was rougher. They ascribed this phenomenon to the higher crystallinity of amylose films due to the starch retrogradation promoted by humidity that lead to a phase separation. The higher roughness of the blends and their nanocomposites compared with that of pure TPS, could be due to the phase separation between EVA and TPS phases. However, a deep study should be done in order to highlight if starch retrogradation is also contributing on the surface roughness of those materials. The surface of the films undergoing biodegradation were highly rough in comparison to the surfaces before being subjected to the biodegradation process. The SEM images revealed that the surfaces of the samples subjected to disintegration under composting conditions is significantly eroded after 18 days, probably due prior to water and then to microorganisms attack (Fig. 7b, h, l, p and t). After 18 days, random degradation produced evident signs of disintegration such as cavities with evident holes on the surface of the films, confirming that the enzymatic degradation is taking place on starch phase. After 56 days and particularly after 150 days of exposition to the composting medium, the voids resulted higher in B40TPS (Fig. 7i and j) and B50TPS (Fig. 7m and n) blends due to the removal of TPS phase during the composting test. In the case of nanocomposites, much and smaller holes were observed at 56 days and particularly at 150 days, confirming that nanoparticles enhanced the compatibility of EVA and TPS matrix [36], leading to a more uniform dispersion of TPS in EVA matrix.
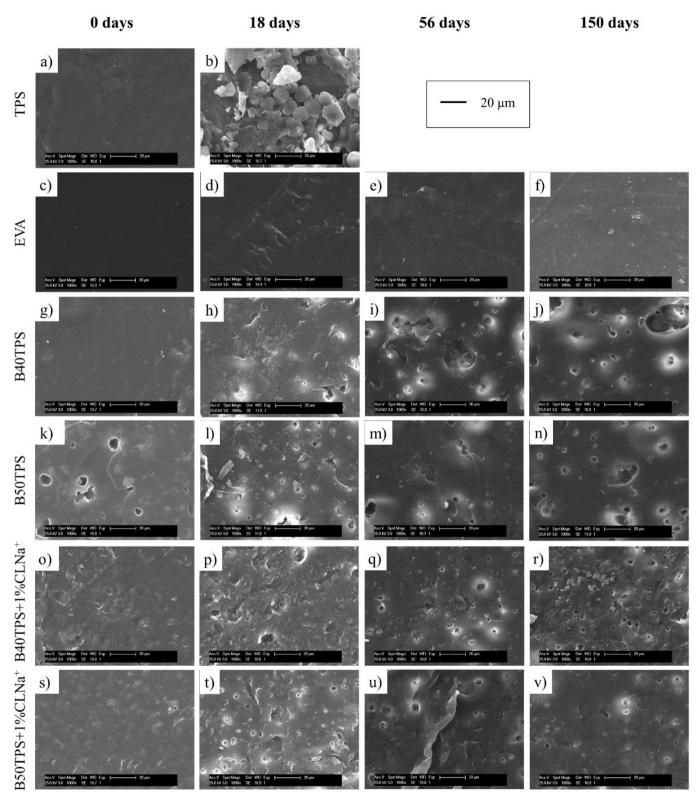
Fig. 7. SEM images of all the samples at different degradation time under composting conditions.

Fig. 8 shows the ATR-FTIR analysis of EVA/TPS blends and their nanocomposite films at different composting times. In the case of neat EVA sample (Fig. 8a), the broad peak related with the free hydroxyl groups (3700-3000 cm^{-1}) increased in intensity during composting, probably related to the formation of hydrogen bonding interaction between the carbonyl group in vinyl acetate and water, due to the increasing water absorption in EVA matrix in composting medium. The bands at 1738 cm^{-1} (asymmetric stretching of the carbonyl group, $-C=O$), at 1650 cm^{-1} (trans-vinylene double bond, $C=C$) and at 1465 cm^{-1} (methylene stretch, $-CH_2$), did not change
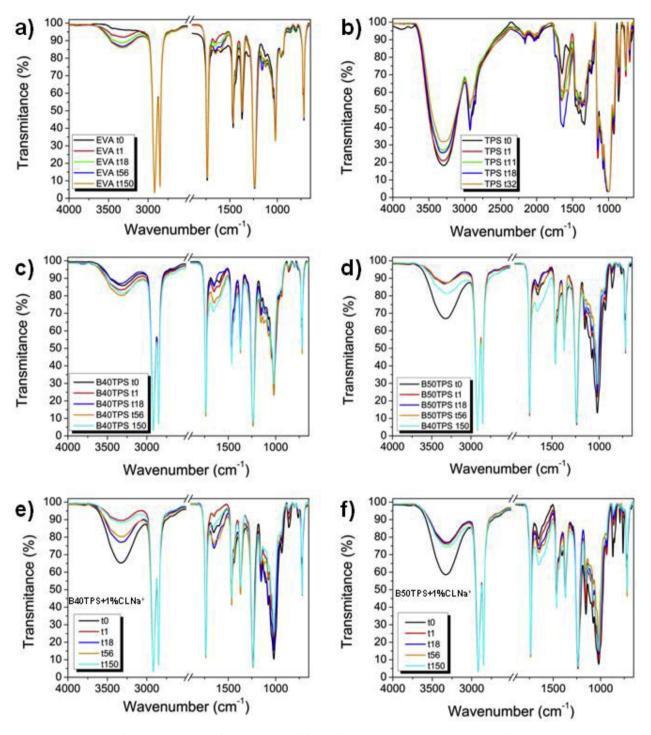
Fig. 8. ATR-FTIR spectra of all the samples at different disintegration times under composting conditions.

with composting times, since EVA is a non-biodegradable polymer. Meanwhile, the band related with C-O-C stretch mode ($1156 \, cm^{-1}$) changed in intensity during composting as it was previously observed in EVA samples during composting test [42]. In neat TPS sample during composting, there is a significant decrease on the intensity of the broad band between 3700 and $3000 \, cm^{-1}$, ascribed to the stretching vibration mode of the hydroxyl group (-OH). This band decreased during composting due to the biodegradation of TPS matrix. Meanwhile, the peak at $1645 \, cm^{-1}$ ascribed to the bending of the -OH group [53] increased during composting as a

consequence of the increasing hydrogen bonding interaction of the remaining -OH groups with the bonded water in the composting medium.

In the case of EVA/TPS blends, the main changes were observed in the bands related with the hydroxyl groups. The intensity of the band related with -OH stretching vibration ($3700 - 3000 \, cm^{-1}$) in B40TPS and its nanocomposite ($B40TPS + CLNa^+$) increased during composting, due to the higher EVA content which did not undergo disintegration in compost and that interacts with water. On the other hand, the band corresponding to the bending mode of starch

-OH group ($1642 \, cm^{-1}$) mainly disappeared with the disintegration of starch matrix. Meanwhile, the band corresponding to the terminal trans-vinylene double bond ($1650 \, cm^{-1}$) increased since EVA did not experimented disintegration. In the case of B50TPS and its nanocomposite (B50TPS + CLNa$^+$) the intensity of the -OH stretching band ($3700 - 3000 \, cm^{-1}$) first showed higher intensity than blends with 40 wt % of TPS, due to the higher TPS content. This band significantly decreased during composting, as a consequence of TPS matrix disintegration from 0 to 56 days. However, at 156 days, this band increased, particularly in B50TPS, due to the EVA matrix interaction with water in compost medium. This result suggests that the nanoparticle are interacting with the polymeric matrix and thus avoiding/reducing the water absorption.

TG and DTG curves (not shown) revealed the changes of the thermal stability due to the disintegration under composting conditions of neat EVA and TPS, EVA/TPS blends and their respective nanocomposites after different disintegration times (before and after composting). The main results are summarized in Table 2. TPS loss indicates the amount of TPS lost after disintegration referred to the total TPS amount presents in the sample before disintegration under composting conditions. These values were calculated from the TG curve of the disintegrated samples taking the drop attributed to TPS degradation.

In Table 2, it is possible to observe that after 150 days of disintegration under composting conditions, TPS is still present in the blends and their nanocomposites. Comparing with neat TPS, which degraded completely after 56 days, TPS in the blends and the nanocomposites is somehow thermally stabilized thanks to the strong interaction with EVA. Indeed, after 150 days under composting conditions there is still high amount of TPS in the blends and their nanocomposites, confirming the previous results obtained by WCA and degree of disintegrability, disintegration test and SEM observation. It was observed that $T_{5\%}$ decreased

significantly ($p > 0.05$) with the disintegration time, while a relative slight decrease was observed for T_{maxTPS}, $T_{maxEVAI}$ and $T_{maxEVAII}$. The high decrease of $T_{5\%}$ ($p > 0.05$) after only 1 day of degradation is probably related with the TPS plasticizer loss caused by hydrolysis during the initial degradation stage. It is interesting to notice from the TPS loss values that for EVA/TPS blends and their nanocomposites, the amount of TPS lost after 1 day is almost the same of samples after 18 days. It means that a part of TPS was degraded since 1 day under composting conditions and the disintegration of the rest of TPS needed more than 18 days to start the degradation process, as it resulted from the weight loss analysis. This is probably due to the recrystallization of the remaining starch under composting conditions as it was previously observed. It is known that the interaction of the plasticizer with starch polymeric chains limits crystal growth and hinders their alignment and recrystallization [71]. In fact, the recrystallization process is caused by the tendency of macromolecules to form hydrogen bonds during the expulsion of plasticizer [72]. It seems that during composting, since the plasticizer was previously hydrolyzed, one fraction of the starchy material started the disintegration while other fraction was able to recrystallize. Considering that amylose recrystallization is faster, it seems that mainly amylopectin fraction of TPS was degraded in 1 day under composting conditions. In fact, it is known that the amylopectin recrystallization is slower and mainly responsible for deterioration of starch [71]. For the other disintegration times, a gradual increase of the TPS loss was observed as the disintegration time increased for all the samples. Slight different behavior was observed for B40TPS + 1% CLNa$^+$, which showed an almost constant TPS loss values even after 56 days of composting test, confirming that nanoparticles enhance the compatibility of EVA and TPS matrix [36] and then confirming the main results obtained in this work. Once more, these results show that partially biodegradable blends were successfully obtained showing higher

Table 2
TG and DTG parameters for all the samples at different disintegration times.

Sample	Degradation time (days)	$T_{5\%}$ (°C)	T_{maxTPS} (°C)	$T_{maxEVAI}$ (°C)	$T_{maxEVAII}$ (°C)	TPS loss (%)
EVA	0	338[a,b]	—	352[a]	465[a]	—
	1	339[a]	—	352[a]	476[b]	—
	18	337[a,b]	—	352[a]	474[b]	—
	56	336[b]	—	352[a]	474[b]	—
	150	337[a,b]	—	351[a]	476[b]	—
TPS	0	255[a]	313[a]	—	—	—
	1	183[b]	294[b]	—	—	—
	11	179[c]	292[b,c]	—	—	—
	18	177[c]	292[b,c]	—	—	—
	32	174[d]	290[c]	—	—	—
B40TPS	0	304[a]	317[a]	368[a]	484[a]	0
	1	273[b]	312[b]	357[b]	476[b]	20
	18	257[c]	309[c]	351[c]	475[b,c]	20
	56	247[d]	298[d]	346[d]	473[c]	28
	150	250[e]	297[d]	351[c]	476[b]	53
B50TPS	0	304[a]	317[a]	363[a]	484[a]	0
	1	267[b]	311[b]	352[b]	476[b]	29
	18	279[c]	316[a]	352[b]	474[b]	30
	56	288[d]	318[a]	354[b]	475[b]	44
	150	234[e]	306[c]	352[b]	474[b]	66
B40TPS+1%CLNa$^+$	0	306[a]	319[a]	367[a]	484[a]	0
	1	240[b]	320[a,b]	361[b]	479[b,c]	22
	18	283[c]	319[a,b]	360[b]	478[b]	25
	56	265[d]	317[a]	359[b]	481[c]	23
	150	275[e]	320[b]	359[b]	478[b]	30
B50TPS+1%CLNa$^+$	0	300[a]	320[a]	369[a]	486[a]	0
	1	272[b]	319[a]	365[b]	478[b]	28
	18	266[c]	319[a]	362[c]	479[b]	28
	56	288[d]	319[a]	362[c]	477[b]	39
	150	221[e]	306[b]	363[b,c]	477[b]	54

[a-e] Different letters within the same column in each formulation indicate significant differences in thermal parameters among degradation days ($p < 0.05$).

values (compared with neat EVA) of disintegrability with higher TPS content, and lower values of disintegrability enhancing the compatibility thanks to the compatibilizing effect of natural bentonite.

4. Conclusions

In this work natural bentonite was used to improve the compatibility of EVA/TPS blends. Although the nanofillers are preferentially located into TPS matrix due to the polar interaction between the silicate layers of natural bentonite and TPS, they also interact at the interface with the VA polar groups of EVA. This was revealed from FE-SEM analysis, showing that nanofillers increase the interfacial adhesion between both phases and leads to an improvement of the compatibility between both polymeric phases avoiding the coalescence of TPS phase into EVA matrix. SEM images showed the immiscibility character of EVA/TPS blends and their nanocomposites. Better dispersion of TPS phase into the EVA matrix was observed for the nanocomposites with a more homogeneous size distribution of the TPS spherical microdomains compared with the neat blends, as well as a strong decrease of the phase debonding, indicating better compatibility between the different polymer phases due to the addition of nanoclays. The TGA showed that thermal degradation of EVA/TPS blends takes place in three main steps, as it was expected for immiscible blends: TPS, vinyl acetate and ethylene degradation, respectively. Moreover, a strong decrease of the $T_{5\%}$ of the blends and their nanocomposites, compared to neat EVA, was observed due to the fast loss of bounded water and plasticizer in the film after 80 °C. In addition, the thermal stability of starch was increased according with the EVA content in the blend. ATR-FTIR analysis showed that the TPS based materials are strongly affected by humidity conditions and static water contact angles revealed that the addition of hydrophilic TPS slightly increased the wettability of EVA in the blends and nanocomposites due to EVA encapsulation of TPS phase leading to a less exposure of starch at the surface. Meanwhile, contact angle hysteresis (WCAH) measurements showed that wettability of EVA/TPS blends increased with water contact cycles, but the WCAH of nanocomposites was maintained during 3 cycles due to better interaction between EVA and TPS thanks to the nanofiller presence. Disintegration tests under composting conditions showed that EVA/TPS blends presented positive interactions, which delay the disintegration of TPS matrix under composting conditions. Higher compatibility was observed by adding natural bentonite, since the nanocomposites experimented lower disintegration during composting and they showed more uniform dispersion of TPS phase into EVA matrix as evidenced by SEM images. The TGA of disintegrated samples shows TPS loss values almost constant for all the samples until 18 days of disintegration test. Nevertheless, higher values of disintegrability were found for higher TPS contents, while lower values of disintegrability were found enhancing the compatibility thanks to the compatibilizing effect of natural bentonite. This work revealed the possibility to easily melt-process EVA/TPS blends with traditional industrial methods, obtaining TPS based materials with enhanced performances for potential industrial applications. Moreover, blending biodegradable polymers such as TPS with non-biodegradable polymers like EVA leads to the increase of compostable polymer percentage in partially-degradable materials giving possible solution for the end-life of these materials after their use.

Acknowledgements

Appendix A. Supplementary data

Supplementary data to this article can be found online at https://doi.org/10.1016/j.polymdegradstab.2018.11.025.

References

[1] J.R. Jambeck, R. Geyer, C. Wilcox, T.R. Siegler, M. Perryman, A. Andrady, et al., Plastic waste inputs from land into the ocean, Science 347 (2015) 768–771.
[2] M.N. Belgacem, A. Gandini, Monomers, Polymers and Composites from Renewable Resources, Elsevier, 2011.
[3] J. Vartiainen, M. Vähä-Nissi, A. Harlin, Biopolymer films and coatings in packaging applications—a review of recent developments, Mater. Sci. Appl. 5 (2014) 708.
[4] A. Wojtowicz, L.P.B.M. Janssen, L. Moscicki, Blends of natural and synthetic polymers, in: L.P.B.M. Janssen, L. Moscicki (Eds.), Thermoplastic Starch: a Green Material for Various Industries. Weinheim, Germany, 2009, pp. 35–53.
[5] R. Muthuraj, M. Misra, A.K. Mohanty, Biodegradable compatibilized polymer blends for packaging applications: a literature review, J. Appl. Polym. Sci. 135 (2018) 45726.
[6] H. Vieyra Ruiz, E.S.M. Martínez, M.A.A. Mendez, Biodegradability of polyethylene–starch blends prepared by extrusion and molded by injection: evaluated by response surface methodology, Starch Staerke 63 (2011) 42–51.
[7] D. Lourdin, L. Coignard, H. Bizot, P. Colonna, Influence of equilibrium relative humidity and plasticizer concentration on the water content and glass transition of starch materials, Polymer 38 (1997) 5401–5406.
[8] B. Khan, M. Bilal Khan Niazi, G. Samin, Z. Jahan, Thermoplastic starch: a possible biodegradable food packaging material—a review, J. Food Process. Eng. 40 (2017) e12447.
[9] M.R. Roslan, N.M. Nasir, E. Cheng, N. Amin, Tissue engineering scaffold based on starch: a review. Electrical, Electronics, and Optimization Techniques (ICEEOT), in: International Conference on: IEEE, 2016, pp. 1857–1860.
[10] Y. Zhang, C. Rempel, Q. Liu, Thermoplastic starch processing and characteristics—a review, Crit. Rev. Food Sci. Nutr. 54 (2014) 1353–1370.
[11] H. Schmitt, A. Guidez, K. Prashantha, J. Soulestin, M. Lacrampe, P. Krawczak, Studies on the effect of storage time and plasticizers on the structural variations in thermoplastic starch, Carbohydr. Polym. 115 (2015) 364–372.
[12] U. Shah, F. Naqash, A. Gani, F.A. Masoodi, Art and science behind modified starch edible films and coatings: a review, Compr. Rev. Food Sci. Food Saf. 15 (2016) 568–580.
[13] N. Masina, Y.E. Choonara, P. Kumar, L.C. du Toit, M. Govender, S. Indermun, et al., A review of the chemical modification techniques of starch, Carbohydr. Polym. 157 (2017) 1226–1236.
[14] C. Menzel, M. Andersson, R. Andersson, J.L. Vázquez-Gutiérrez, G. Daniel, M. Langton, et al., Improved material properties of solution-cast starch films: effect of varying amylopectin structure and amylose content of starch from genetically modified potatoes, Carbohydr. Polym. 130 (2015) 388–397.
[15] N. Karaki, A. Aljawish, C. Humeau, L. Muniglia, J. Jasniewski, Enzymatic modification of polysaccharides: mechanisms, properties, and potential applications: a review, Enzym. Microb. Technol. 90 (2016) 1–18.
[16] R. Ortega-Toro, J. Bonilla, P. Talens, A. Chiralt, Future of Starch-based Materials in Food Packaging. Starch-based Materials in Food Packaging, Elsevier, 2018, pp. 257–312.
[17] D.M. Nguyen, T.V.V. Do, A.-C. Grillet, H.H. Thuc, C.N.H. Thuc, Biodegradability of polymer film based on low density polyethylene and cassava starch, Int. Biodeterior. Biodegrad. 115 (2016) 257–265.
[18] R. Ortega-Toro, J. Contreras, P. Talens, A. Chiralt, Physical and structural properties and thermal behaviour of starch-poly (ε-caprolactone) blend films for food packaging, Food Packag. Shelf Life 5 (2015) 10–20.
[19] E. Schwach, L. Averous, Starch-based biodegradable blends: morphology and interface properties, Polym. Int. 53 (2004) 2115–2124.
[20] A.M. Peres, R.R. Pires, R.L. Oréfice, Evaluation of the effect of reprocessing on the structure and properties of low density polyethylene/thermoplastic starch blends, Carbohydr. Polym. 136 (2016) 210–215.
[21] J. Ferri, D. Garcia-Garcia, L. Sánchez-Nacher, O. Fenollar, R. Balart, The effect of maleinized linseed oil (MLO) on mechanical performance of poly (lactic acid)-thermoplastic starch (PLA-TPS) blends, Carbohydr. Polym. 147 (2016) 60–68.
[22] J. Muller, C. González-Martínez, A. Chiralt, Combination of poly (lactic) acid and starch for biodegradable food packaging, Materials 10 (2017) 952.
[23] K.A. Garrido-Miranda, B.L. Rivas, M.A. Pérez-Rivera, E.A. Sanfuentes, C. Peña-Farfal, Antioxidant and antifungal effects of eugenol incorporated in bio-nanocomposites of poly (3-hydroxybutyrate)-thermoplastic starch, LWT 98 (2018) 260–267.

[24] M. Samper, D. Bertomeu, M. Arrieta, J. Ferri, J. López-Martínez, Interference of biodegradable plastics in the polypropylene recycling process, Materials 11 (2018) 1886.

[25] A.L. Da Róz, A.M. Ferreira, F.M. Yamaji, A.J.F. Carvalho, Compatible blends of thermoplastic starch and hydrolyzed ethylene-vinyl acetate copolymers, Carbohydr. Polym. 90 (2012) 34—40.

[26] O. Persenaire, J.M. Raquez, L. Bonnaud, P. Dubois, Tailoring of Co-continuous polymer blend morphology: joint action of nanoclays and compatibilizers, Macromol. Chem. Phys. 211 (2010) 1433—1440.

[27] D. Nguyen, T. Vu, A.-C. Grillet, H.H. Thuc, C.H. Thuc, Effect of organoclay on morphology and properties of linear low density polyethylene and Viet-namese cassava starch biobased blend, Carbohydr. Polym. 136 (2016) 163—170.

[28] M. Samper-Madrigal, O. Fenollar, F. Dominici, R. Balart, J. Kenny, The effect of sepiolite on the compatibilization of polyethylene—thermoplastic starch blends for environmentally friendly films, J. Mater. Sci. 50 (2015) 863—872.

[29] K.A. Garrido-Miranda, L. Rivas B, M.A. Pérez, Poly (3-hydroxybutyrate)—thermoplastic starch—organoclay bionanocomposites: surface properties, J. Appl. Polym. Sci. 134 (2017) 45217.

[30] D.A. D'Amico, R.P. Ollier, V.A. Alvarez, W.F. Schroeder, V.P. Cyras, Modification of bentonite by combination of reactions of acid-activation, silylation and ionic exchange, Appl. Clay Sci. 99 (2014) 254—260.

[31] A.M. Henderson, Ethylene-vinyl acetate (EVA) copolymers: a general review, IEEE Electr. Insul. Mag. 9 (1993) 30—38.

[32] C. Schneider, R. Langer, D. Loveday, D. Hair, Applications of ethylene vinyl acetate copolymers (EVA) in drug delivery systems, J. Contr. Release 262 (2017) 284—295.

[33] S. Giri, C. Wan, Electronic Applications of Ethylene Vinyl Acetate and its Composites. Flexible and Stretchable Electronic Composites, Springer, 2016, pp. 61—85.

[34] J. Prinos, D. Bikiaris, S. Theologidis, C. Panayiotou, Preparation and charac-terization of LDPE/starch blends containing ethylene/vinyl acetate copolymer as compatibilizer, Polym. Eng. Sci. 38 (1998) 954—964.

[35] V. Sessini, J.-M. Raquez, G. Lo Re, R. Mincheva, J.M. Kenny, P. Dubois, et al., Multiresponsive shape memory blends and nanocomposites based on starch, ACS Appl. Mater. Interfaces 8 (2016) 19197—19201.

[36] V. Sessini, J.M. Raquez, D. Lourdin, J.E. Maigret, J.M. Kenny, P. Dubois, L. Peponi, Humidity-activated shape memory effects on thermoplastic starch/EVA blends and their compatibilized nanocomposites, Macromol. Chem. Phys. 28 (24) (2017), 1700388.

[37] J.M. Raquez, A. Bourgeois, H. Jacobs, P. Degée, M. Alexandre, P. Dubois, Oxidative degradations of oxodegradable LDPE enhanced with thermoplastic pea starch: thermo-mechanical properties, morphology, and UV-ageing studies, J. Appl. Polym. Sci. 122 (2011) 489—496.

[38] U.-E. Plastics, Determination of the Degree of Disintegration of Plastic Mate-rials under Simulated Composting Conditions in a Laboratory-scale Test. (ISO20200:2015), 2016.

[39] E. Fortunati, S. Rinaldi, M. Peltzer, N. Bloise, L. Visai, I. Armentano, et al., Nano-biocomposite films with modified cellulose nanocrystals and synthesized silver nanoparticles, Carbohydr. Polym. 101 (2014) 1122—1133.

[40] J. González-Ausejo, E. Sanchez-Safont, J.M. Lagaron, R.T. Olsson, J. Gamez-Perez, L. Cabedo, Assessing the thermoformability of poly (3-hydroxybutyrate-co-3-hydroxyvalerate)/poly (acid lactic) blends compatibi-lized with diisocyanates, Polym. Test. 62 (2017) 235—245.

[41] M. Arrieta, V. Sessini, L. Peponi, Biodegradable poly (ester-urethane) incor-porated with catechin with shape memory and antioxidant activity for food packaging, Eur. Polym. J. 94 (2017) 111—124.

[42] E. Fortunati, D. Puglia, J.M. Kenny, M.M.-U. Haque, M. Pracella, Effect of ethylene-co-vinyl acetate-glycidylmethacrylate and cellulose microfibers on the thermal, rheological and biodegradation properties of poly (lactic acid) based systems, Polym. Degrad. Stabil. 98 (2013) 2742—2751.

[43] M.P. Arrieta, M.D. Samper, M. Aldas, J. López, On the use of PLA-PHB blends for sustainable food packaging applications, Materials 10 (2017) 1008.

[44] U. Nöchel, U.N. Kumar, K. Wang, K. Kratz, M. Behl, A. Lendlein, Triple-shape effect with adjustable switching temperatures in crosslinked poly [ethylene-co-(vinyl acetate)], Macromol. Chem. Phys. 215 (2014) 2446—2456.

[45] H.-M. Park, W.-K. Lee, C.-Y. Park, W.-J. Cho, C.-S. Ha, Environmentally friendly polymer hybrids Part I Mechanical, thermal, and barrier properties of ther-moplastic starch/clay nanocomposites, J. Mater. Sci. 38 (2003) 909—915.

[46] M.S. de Luna, G. Filippone, Effects of nanoparticles on the morphology of immiscible polymer blends—challenges and opportunities, Eur. Polym. J. 79 (2016) 198—218.

[47] C. Véchambre, L. Chaunier, D. Lourdin, Novel shape-memosry materials based

[48] J. Parameswaranpillai, S. Thomas, Y. Grohens, Polymer blends: state of the art, new challenges, and opportunities, Char. Polym. Blends (2014) 1—6.

[49] V. Sessini, M.P. Arrieta, J.M. Kenny, L. Peponi, Processing of edible films based on nanoreinforced gelatinized starch, Polym. Degrad. Stabil. 132 (2016) 157—168.

[50] X. Liu, Y. Wang, L. Yu, Z. Tong, L. Chen, H. Liu, et al., Thermal degradation and stability of starch under different processing conditions, Starch Staerke 65 (2013) 48—60.

[51] N.L. García, L. Ribba, A. Dufresne, M. Aranguren, S. Goyanes, Effect of glycerol on the morphology of nanocomposites made from thermoplastic starch and starch nanocrystals, Carbohydr. Polym. 84 (2011) 203—210.

[52] P. González Seligra, L. Eloy Moura, L. Famá, J.I. Druzian, S. Goyanes, Influence of incorporation of starch nanoparticles in PBAT/TPS composite films, Polym. Int. 65 (2016) 938—945.

[53] M. Moreno-Chulim, F. Barahona-Perez, G. Canche-Escamilla, Biodegradation of starch and acrylic-grafted starch by Aspergillus Niger, J. Appl. Polym. Sci. 89 (2003) 2764—2770.

[54] W. Shujun, Y. Jiugao, Y. Jinglin, Preparation and characterization of compatible and degradable thermoplastic starch/polyethylene film, J. Polym. Environ. 14 (2006) 65—70.

[55] O. Yilmaz, C. Cheaburu, D. Durraccio, G. Gulumser, C. Vasile, Preparation of stable acrylate/montmorillonite nanocomposite latex via in situ batch emul-sion polymerization: effect of clay types, Appl. Clay Sci. 49 (2010) 288—297.

[56] F.A. Aouada, L.H. Mattoso, E. Longo, Enhanced bulk and superficial hydro-phobicities of starch-based bionanocomposites by addition of clay, Ind. Crop. Prod. 50 (2013) 449—455.

[57] B. Suresh, S. Maruthamuthu, A. Khare, N. Palanisamy, V. Muralidharan, R. Ragunathan, et al., Influence of thermal oxidation on surface and thermo-mechanical properties of polyethylene, J. Polym. Res. 18 (2011) 2175—2184.

[58] Y. Yuan, T.R. Lee, Contact Angle and Wetting Properties. Surface Science Techniques, Springer, 2013, pp. 3—34.

[59] V. Sessini, M.P. Arrieta, A. Fernández-Torres, L. Peponi, Humidity-activated shape memory effect on plasticized starch-based biomaterials, Carbohydr. Polym. 179 (2018) 93—99.

[60] T.J. Gutiérrez, R. Ollier, V.A. Alvarez, Surface Properties of Thermoplastic Starch Materials Reinforced with Natural Fillers. Functional Biopolymers, Springer, 2018, pp. 131—158.

[61] Å. Rindlav-Westling, M. Stading, P. Gatenholm, Crystallinity and morphology in films of starch, amylose and amylopectin blends, Biomacromolecules 3 (2002) 84—91.

[62] M. Stading, Å. Rindlav-Westling, P. Gatenholm, Humidity-induced structural transitions in amylose and amylopectin films, Carbohydr. Polym. 45 (2001) 209—217.

[63] T.J. Gutiérrez, G. González, Effects of exposure to pulsed light on surface and structural properties of edible films made from cassava and taro starch, Food Bioprocess Technol. 9 (2016) 1812—1824.

[64] G. Kale, T. Kijchavengkul, R. Auras, M. Rubino, S.E. Selke, S.P. Singh, Com-postability of bioplastic packaging materials: an overview, Macromol. Biosci. 7 (2007) 255—277.

[65] P. Sangwan, E. Petinakis, K. Dean, Effects of Formulation, Structure, and Pro-cessing on Biodegradation of Starches. Starch Polymers, Elsevier, 2014, pp. 357—378.

[66] M.P. Arrieta, J. López, E. Rayón, A. Jiménez, Disintegrability under composting conditions of plasticized PLA—PHB blends, Polym. Degrad. Stabil. 108 (2014) 307—318.

[67] V. Siracusa, P. Rocculi, S. Romani, M. Dalla Rosa, Biodegradable polymers for food packaging: a review, Trends Food Sci. Technol. 19 (2008) 634—643.

[68] D.S. Chaudhary, B.P. Adhikari, Understanding polymeric amylose retrograda-tion in presence of additives, J. Appl. Polym. Sci. 115 (2010) 2703—2709.

[69] B.S. Chiou, D. Wood, E. Yee, S.H. Imam, G.M. Glenn, W.J. Orts, Extruded starch—nanoclay nanocomposites: effects of glycerol and nanoclay concen-tration, Polym. Eng. Sci. 47 (2007) 1898—1904.

[70] Å. Rindlav-Westling, P. Gatenholm, Surface composition and morphology of starch, amylose, and amylopectin films, Biomacromolecules 4 (2003) 166—172.

[71] C.M. Jaramillo, T.J. Gutiérrez, S. Goyanes, C. Bernal, L. Famá, Biodegradability and plasticizing effect of yerba mate extract on cassava starch edible films, Carbohydr. Polym. 151 (2016) 150—159.

[72] T. Niranjana Prabhu, K. Prashantha, A review on present status and future challenges of starch based polymer films and their composites in food pack-aging applications, Polym. Compos. 39 (2018) 2499—2522.